Optics Communications 281 (2008) 4499–4503

Contents lists available at ScienceDirect

Optics Communications

journal homepage: www.elsevier.com/locate/optcom

Two-color pulse compression in aperiodically-poled lithium niobate

Xianglong Zeng [a,b,*], Satoshi Ashihara [c,d], Xianfeng Chen [e], Tsutomu Shimura [a], Kazuo Kuroda [a]

[a] Institute of Industrial Science, The University of Tokyo, 4-6-1, Komaba, Meguro-ku, Tokyo 153-8505, Japan
[b] The Key Lab of Specialty Fiber Optics and Optical Access Network, SCIE, Shanghai University, 149 Yanchang Road, Shanghai 200072, China
[c] Department of Applied Physics, Faculty of Engineering, Tokyo University of Agriculture and Technology, 2-24-16 Nakacho, Koganei, Tokyo 184-8588, Japan
[d] PRESTO, Japan Science and Technology Agency (JST), 4-1-8 Honcho, Kawaguchi-shi, Saitama 332-0012, Japan
[e] Department of Physics, Shanghai Jiao Tong University, 800 Dongchuan Road, Shanghai 200240, China

ARTICLE INFO

Article history:
Received 17 January 2008
Received in revised form 30 April 2008
Accepted 30 April 2008

PACS:
42.50.Md
42.65.Re
42.70.Mp

Keywords:
Quadratic solitons
Pulse compression
Group-velocity matching

ABSTRACT

We experimentally demonstrate engineerable compression of two-colored pulses in a linearly-chirped quasi-phase-matching grating. Quadratic solitons generated from fundamental input are reshaped through cascaded parametric processes of second-harmonic generation (SHG) and the back-conversion. We use type-I (e: o + o) SHG geometry in a 50-mm-long aperiodically-poled MgO:$LiNbO_3$ device to satisfy the group-velocity matching condition. Simultaneously compressed fundamental and SH pulses of about 55-fs duration with small pedestal are generated from the fundamental input pulses of 95-fs duration.

1. Introduction

Cascading of quadratic nonlinearity mimics cubic nonlinearity and generates large nonlinear phase shift [1]. Typical geometry is the phase-mismatched second-harmonic generation (SHG), where the periodic back-conversion from the second-harmonic (SH) wave induces intensity-dependent phase shift on the fundamental-frequency (FF) wave. Because each process is usually non-resonant, the cascading nonlinearity provides an alternative way to ultrashort pulse control. Similar to the self-phase modulation in cubic nonlinear media, the cascading nonlinear phase shift can compensate the dispersive broadening or even compress the temporal duration of the FF pulse. Because the sign and the magnitude of the cascading nonlinearity are controllable with the wave-vector mismatch [1], soliton-like propagation and pulse compression can be achieved in either of normal and anomalous dispersion.

A major obstacle in this type of pulse compressor is the group-velocity (GV) mismatch between FF and SH pulses. It reduces the nonlinear phase shift and distorts the temporal phase profile, resulting in degraded compression ratio. We can suppress the phase distortion at the expense of nonlinearity, by exploiting large phase-mismatch condition, where the back-conversion length is shorter than the GV-mismatch length [2]. Soliton-like compression of a FF pulse in normal dispersion region has been demonstrated by use of the self-defocusing nonlinearity at large phase-mismatch condition [2–4]. Recently, the cascading pulse compressor has generated few-cycle FF pulses [5,6]. High compression ratio, however, is inevitably accompanied by degraded pulse quality [3,5].

Soliton excitation is a powerful way to obtain pulses with excellent quality. Optical solitons in quadratic nonlinear media are multi-colored and exist in temporal and/or spatial domain [1,7–9]. Cascaded parametric interactions between FF and SH waves modulate their amplitude and phase in a nonlinear manner, leading to mutual trapping as well as compensation of dispersive/diffractive broadening. It is known that the energy ratio of FF and SH waves as well as their beam widths (or pulse durations in time domain) depends on the phase mismatch and the total energy that they carry [2]. Torner et al. [10] proposed the idea to shape the quadratic solitons to different beam profiles and different energy fraction ratio, by use of aperiodic quasi-phase-matching (QPM) gratings. Here the quadratic solitons, owing to their stability [11,12],

* Corresponding author. Address: The Key Lab of Specialty Fiber Optics and Optical Access Network, SCIE, Shanghai University, 149 Yanchang Road, Shanghai 200072, China.
E-mail address: zenglong@shu.edu.cn (X. Zeng).

0030-4018/$ - see front matter
doi:10.1016/j.optcom.2008.04.080

adiabatically adapt themselves to the soliton solutions according to the local wave-vector mismatch. Carrasco et al. numerically showed that spatial solitons are excited with enhanced efficiency by use of synthetic phase-matching profiles [13]. Spatial soliton families have been experimentally excited in engineered QPM gratings so far [14].

Although the governing equation of the quadratic soliton is similar between space and time domain, the excitation of temporal soliton is not straightforward. The experiments are usually encountered by the GV mismatch, which disturbs the soliton formation. If the GV mismatch is intrinsically or reduced to be small, the nonlinearity is enhanced and excitation of two-colored temporal solitons becomes possible [15]. Recent developments in the GV-matching scheme available with QPM devices [16–20] can potentially open the way to the engineerable excitation of the two-colored temporal solitons. Non-adiabatic compression of FF and SH pulses has been demonstrated by use of GV-matched SHG geometry in 10-mm-long periodically poled MgO-doped lithium niobate (PPMgLN) [21]. Recently, we have numerically shown that the adiabatic compression becomes possible by exploiting GV-matched configurations in QPM devices [22]. Here the input FF pulse is adiabatically reshaped into the two-colored soliton with excellent profiles and short durations.

In this Letter, we present what we believe the first experimental demonstration of two-colored pulse compression in a chirped QPM grating. The input FF pulse is transformed into two-colored soliton with shorter temporal durations in an engineered manner. We also discuss spatial distribution of the compression properties with numerical simulations.

2. Experiment

Let us briefly review how to realize adiabatic or engineered compression of two-colored temporal soliton (for details, see Ref. [22]). We consider a chirped QPM grating, where the local effective wave-vector mismatch varies along the propagation direction. The (effective) wave-vector mismatch $\Delta k(z) = k_2 - 2k_1 - 2\pi/\Lambda(z)$ is determined by the local domain reversal period $\Lambda(z)$, where k_1 and k_2 are the wave number at the center wavelength of FF and SH pulses, respectively. Because of the stability of quadratic solitons, the FF and SH pulses dynamically adapt themselves to the soliton solutions according to the local wave-vector mismatch $\Delta k(z)$. In fact, the properties of quadratic soliton, the energy ratio of FF and SH waves as well as their pulse durations depends on the wave-vector mismatch. If we design the longitudinal distribution of the wave-vector mismatch properly, both FF and SH pulses may have shorter pulse duration at the exit of the device, compared with the input FF pulse.

We performed the experiments by use of aperiodically-poled 5-mol% MgO-doped lithium niobate (APPMgLN). As is schematically shown in Fig. 1, type-I (e: o + o) geometry via the off-diagonal nonlinear coefficient d_{32} is utilized to satisfy the GV-matching between FF and SH pulses for the FF wave at the communication band [16]. The APPMgLN device has 1-mm thickness and a linearly-chirped grating whose poling period Λz varying from 19.9 μm to 20.4 μm (HC Photonics Corp., Taiwan). The total device length L is 50 mm, which corresponds to 2.2 (4.5) times the dispersion length of a 95-fs FF (SH) pulses. Here we note that the material has the group-velocity dispersion of positive sign (normal dispersion) at both the FF and SH wavelengths. Therefore the sign of the nonlinear phase shifts accumulated during the cascaded parametric interactions should be negative (or self-defocusing nonlinearity) for soliton generation and compression.

The fundamental pulse with duration of 95 fs in full width at half minimum (FWHM) and the center wavelength of 1570 nm is generated from optical parametric amplifier pumped by a regeneratively amplified Ti:sapphire laser. The fundamental beam is focused to have beam diameter of 350 μm (FWHM) at the waist by using a lens of 300-mm focal length. In order to compensate the self-defocusing along propagation, we place the device at the converging side of the beam such that the output face of the device exists at the beam focus (see Fig. 1). The temperature of the whole device is controlled homogeneously within an accuracy of 0.1 °C.

From the temperature-dependent Sellmeier formula [23], we deduce $\delta k/\delta T = 0.343\ \mathrm{mm^{-1}\,K^{-1}}$ for the temperature range of 25–60 °C. The temperature dependence of the local effective wave-vector mismatch for the center wavelength 1570 nm is represented as $\Delta k(T,z) = (T - T_{\mathrm{QPM}}) * \delta k/\delta T + \Delta k(T_{\mathrm{QPM}}, z = 0) * ((L - z)/L)$, where z is the coordinate along the propagation direction. The QPM temperature, T_{QPM}, for the QPM period of 20.4 μm at the FF wavelength of 1570 nm is experimentally found to be 38.0 °C: we measured the FF depletion in a 50-mm-long periodical-poled grating of 20.4-μm period, which is fabricated aside the chirped grating on the same wafer. If we set the device temperature as $T = T_{\mathrm{QPM}}$, the wave-vector mismatch $\Delta k(T_{\mathrm{QPM}}, 0)$ at the entrance face ($z = 0$, $\Lambda_0 = 19.9$ μm) equals to 7.5 $\mathrm{mm^{-1}}$, whereas that at the exit face, $\Delta k_L(T_{\mathrm{QPM}}) = \Delta k(T_{\mathrm{QPM}}, L)$ equals to 0 $\mathrm{mm^{-1}}$. We measured the pulse energy and the duration while changing the device temperature. When we present the temperature dependences in the following, we plot the results as functions of the effective wave-vector mismatch at the exit face $\Delta k_L(T)$.

3. Results and discussion

Fig. 2a shows the fundamental transmittance for input peak intensities of 20 and 25 $\mathrm{GW/cm^2}$, respectively, as functions of the Δk_L. Simulated results are also plotted as solid and dashed lines.

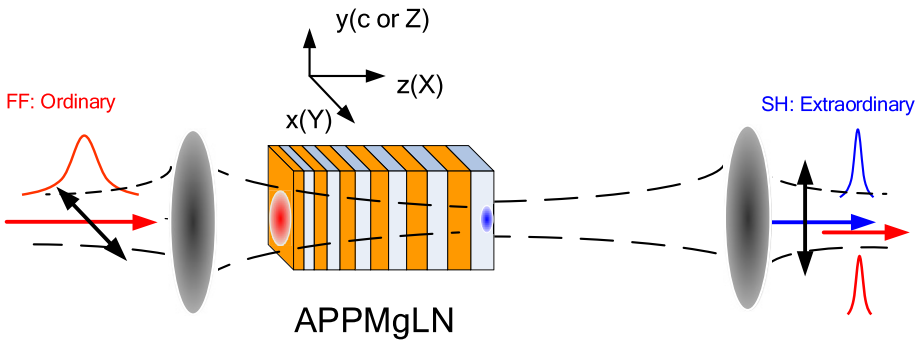

Fig. 1. Schematic of the adiabatic compression in aperiodically-poled MgO-doped lithium niobate (APPMgLN). Our laboratory coordinate (x, y, z) corresponds to the crystallographic axis of (Y, Z or c, X), respectively.

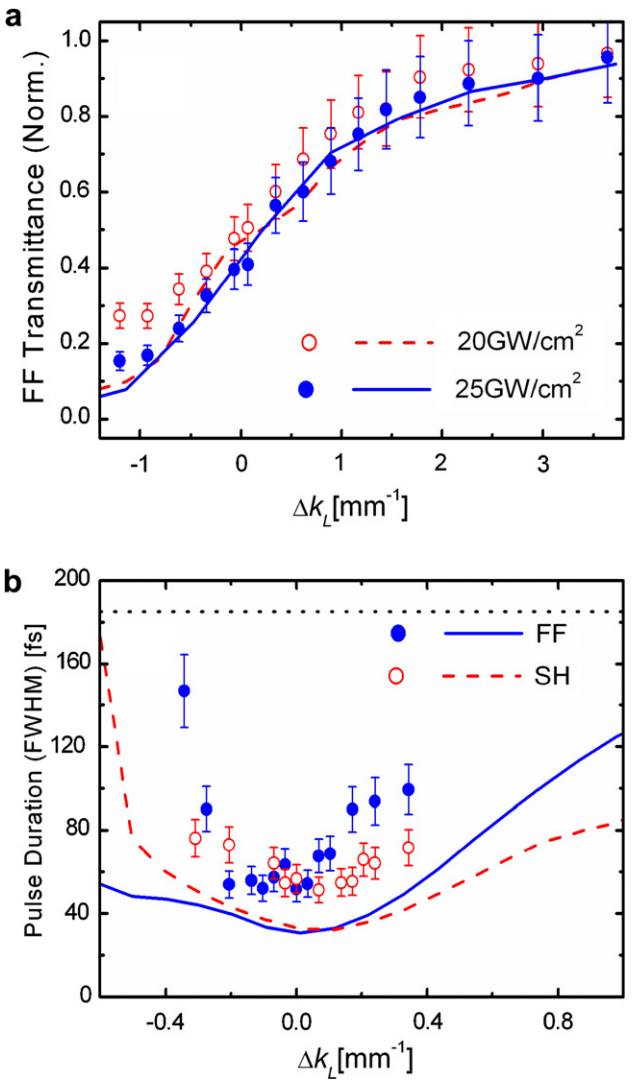

Fig. 2. (a) Measured fundamental transmittance for pump intensities of 20 and 25 GW/cm^2 as functions of $\Delta k_L(T)$. (b) The temporal durations of FF and SH pulses for pump intensity of 20 GW/cm^2 as functions of $\Delta k_L(T)$. Numerical results are shown as dashed and solid lines. The dotted line in (b) represents the dispersive spreading of the FF pulse in the linear limit.

Here we numerically solve the coupled-wave equations by using one-dimensional split-step beam propagation method (BPM) under the plane-wave approximation. Agreement between the experiments and the numerical simulations is fairly well. The pulse energies of FF and SH are almost equal when the device temperature is set such that the QPM condition is satisfied at the exit face, namely, $\Delta k_L(T) = 0$.

The intensity autocorrelation traces of the output FF and SH pulses are measured at different device temperatures. The FWHM durations for the input peak intensity of 20 GW/cm^2, deduced by assuming sech^2-shape, are plotted in Fig. 2b as functions of $\Delta k_L(T)$. We note here that pulse narrowing occurs both at positive and negative signs of $\Delta k_L(T)$. This is not surprising because the soliton families indeed exist at both positive and negative wave-vector mismatches (see for example Ref. [9]). The sign of the nonlinear phase shift, which depends on the phase-relationship between FF and SH waves as well as on the wave-vector mismatch Δk, is negative even for negative Δk in the current case. Here the wave-vector mismatch $\Delta k(z) = k_2 - 2k_1 - 2\pi\Lambda(z)$ is determined only by the domain reversal period and does not include the effect coming from the nonlinear phase shift. Note that we plot the pulse duration for limited range in Fig. 2b compared with Fig. 2a. The dotted line represents the output pulse duration of a FF pulse in the linear limit: the FF pulse broadens to be 185 fs because of the group-velocity dispersion in the 50-mm-long device in the absence of nonlinearity (see Fig. 3a). If the cascading nonlinearity emerges, two-colored pulses mimic the adiabatic shaping processes and approach the soliton solution according to the local wave-vector mismatch. The simultaneously compressed FF and SH pulses of 57 and 54 fs duration are generated with small pedestal at $0 < \Delta k_L < 0.1$ mm^{-1}. Numerical results obtained from 1D-BPM simulations are shown as solid (FF) and dashed (SH) lines, respectively. Although the simulations expect even shorter pulses (~40 fs), the Δk_L-dependence of the output pulse durations are common between experiments and simulations.

Fig. 3a and b shows the measured intensity autocorrelation traces of the output FF and SH pulses for Δk_L ($T = 38.3$ °C) = 0.07 mm^{-1} and the pump intensity of 20 GW/cm^2. The autocorrelation measurements are performed without any kind of pin-hole in front of the autocorrelator: the spatial non-uniformity, if there exists, is averaged out in the measurement. As we see here, simultaneously compressed FF and SH pulses with temporal duration of 57 and 55 fs are obtained with only a slight

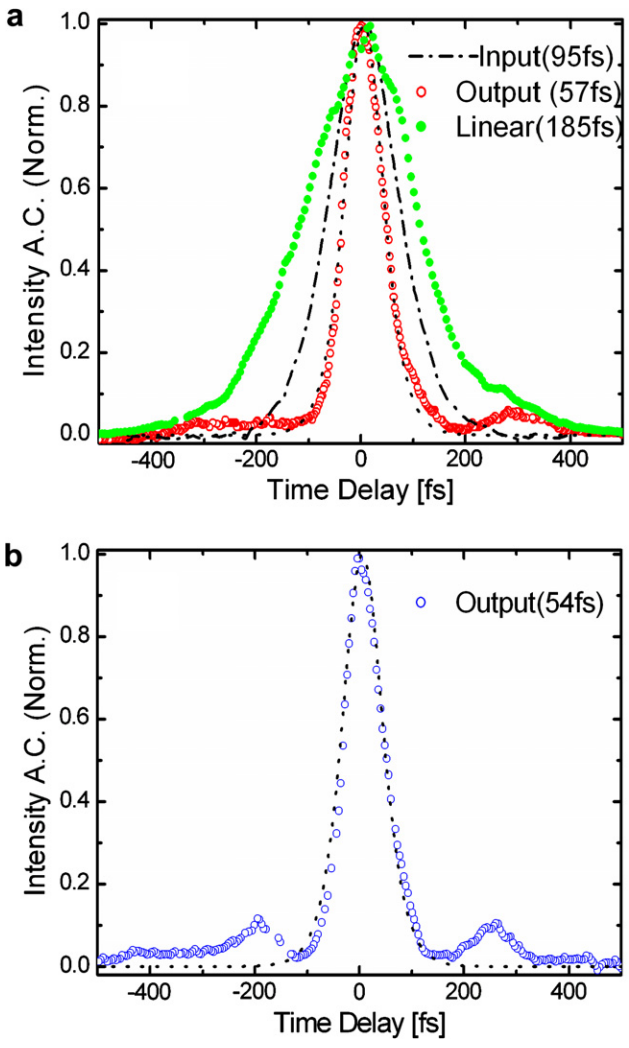

Fig. 3. Measured intensity autocorrelation traces of (a) the input pulse (dash-dotted line), the output FF (open circle), and (b) the output SH pulses (open circle), obtained at $\Delta k_L = 0.07$ mm^{-1}. The output FF pulse in the linear propagation limit is shown as filled circle in (a). Dashed lines in (a) and (b) are the sech^2-shaped fitted curves.

fraction of pedestal. The measurement is also performed for the FF pulse in the linear regime (large phase mismatch and small intensity) and plotted as filled circles in Fig. 3a. The measured dispersive broadening up to ~185 fs agrees well with theory: simple calculation of the dispersive broadening of a FF pulse with 95-fs duration in its transform-limit suggests the output pulse duration of 180 fs. In order to estimate the quality of the compressed pulses, we define a quality factor of an autocorrelation (not the pulse shape itself): we fit the autocorrelation traces with a Gaussian function, and calculate the fractional amount of the central spike normalized by the total amount. The calculated quality factors for FF and SH pulses are 90.4 % and 88.5%, respectively. Although the observed compression ratio is not as large as expected, the compressed pulse duration is still more than 3 times shorter than 185 fs, which would result from the dispersive broadening in the linear regime. This fact suggests the successful realization of the shaping of two-colored pulses in an engineered QPM grating.

Fig. 4a and b shows the measured intensity spectra of the input FF, the output FF and the output SH pulses, respectively. Both FF and SH spectra become broadened without frequency shift. The absence of frequency shift implies that the GV mismatch is negligible. The temporal profiles and the intensity autocorrelations are calculated assuming transform-limited pulses from the measured spectra and shown in Fig. 4c and d. The corresponding pulse duration is 42 fs (FF) and 45 fs (SH). The difference in the autocorrelation traces between the direct measurement and the Fourier transformation of the spectrum implies the existence of chirp for the output FF and SH pulses. A phase-sensitive measurement, such as the FROG method, is required to make this point clearer. Here we note that the broadened spectral profiles have some structure, which shows the deviation from ideal adiabatic shaping. The pulses experience some oscillations both in temporal and spectral profiles. The oscillation firstly may come from the transformation from one input FF pulse to quadratic solitons at finite Δk value in the beginning stage of pulse propagation. In addition, the spectral profiles may oscillate around the stationary solutions along propagation because of the spatial variation of the QPM period. For comparison, numerical results (1D-BPM) obtained by using the same input pulse and device parameters are shown as dash-dotted lines. Some pedestals are also observable in the simulation results, although the pulse durations are narrower. The unwanted oscillations would be reduced and the compressed pulses would become pedestal-free if we use the device with longer interaction length, where the QPM period starts with larger Δk value and varies more moderately [13,22].

The quantitative deviation with regard to the compressed pulse durations between our experiments and theory, as shown in Fig. 2b, may come from the imperfection of the QPM grating and the spatially non-uniform nonlinear dynamics. As is usually the case, the reversed domain pattern of our device is not perfectly identical between the top ($+z$) and the bottom ($-z$) surfaces. In our experiments with the bulk device, the spectrum or the temporal profile can be spatially non-uniform because the input FF pulse has spatial intensity distribution of Gaussian shape and the cascading nonlinearity is intensity-dependent. In order to investigate the spatio-temporal dynamics, we solve the standard (2+1)D (1-temporal, 1-spatial and propagation axis) coupled-wave equations. Although (3+1)D simulations describe our experiments more precisely, we chose (2+1)D simulations to save the memory size as well as the calculation time. We consider the same QPM design and the device size as those in our experiments. It is assumed that the input FF beam is collimated with the FWHM width of 350 μm. The calculated spatial–temporal intensity profile of the output FF pulse is shown in Fig. 5a. Here we use the peak intensity of 20 GW/cm^2 and the temperature corresponding to $\Delta k_L = 0$. We can see that the pulse at the center of the beam is well-compressed, while the pulse at the edge is not. This clearly comes from the spatial intensity distribution and the resulting spatially-dependent nonlinearity. In simulations, cubic nonlinearity is taken in account. The cubic nonlinearity counteracts with the cascading self-defocusing nonlinearity, which trend becomes enhanced at higher intensity because of the saturable nature of the cascading nonlin-

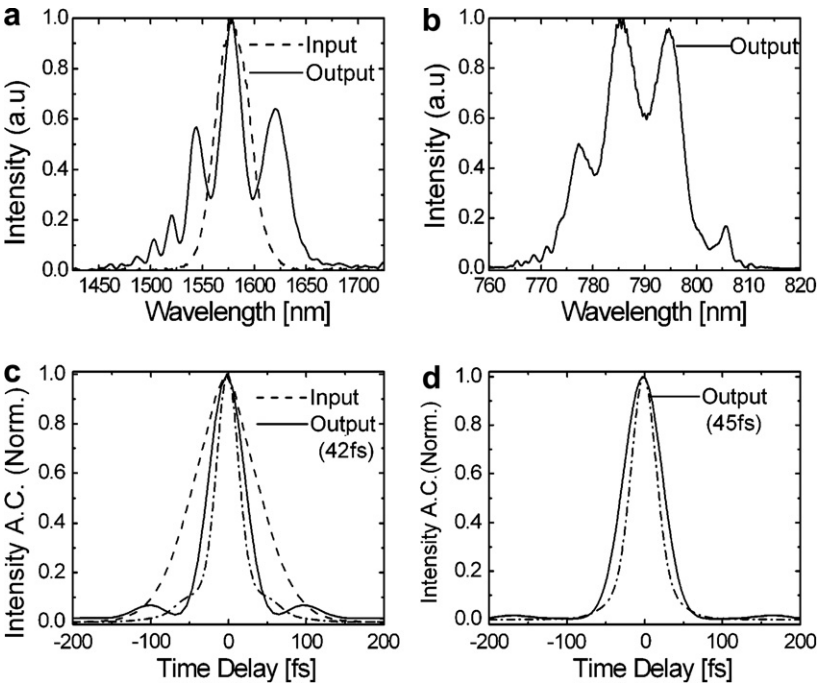

Fig. 4. Measured intensity spectra of (a) the input FF (dashed), the output FF (solid), and (b) the output SH pulses. Intensity autocorrelation traces calculated from the measured spectra are shown for (c) the input FF (dashed), the output FF (solid), and (d) the output SH pulses, respectively. Numerical results (1D-BPM) are shown as dash-dotted lines.

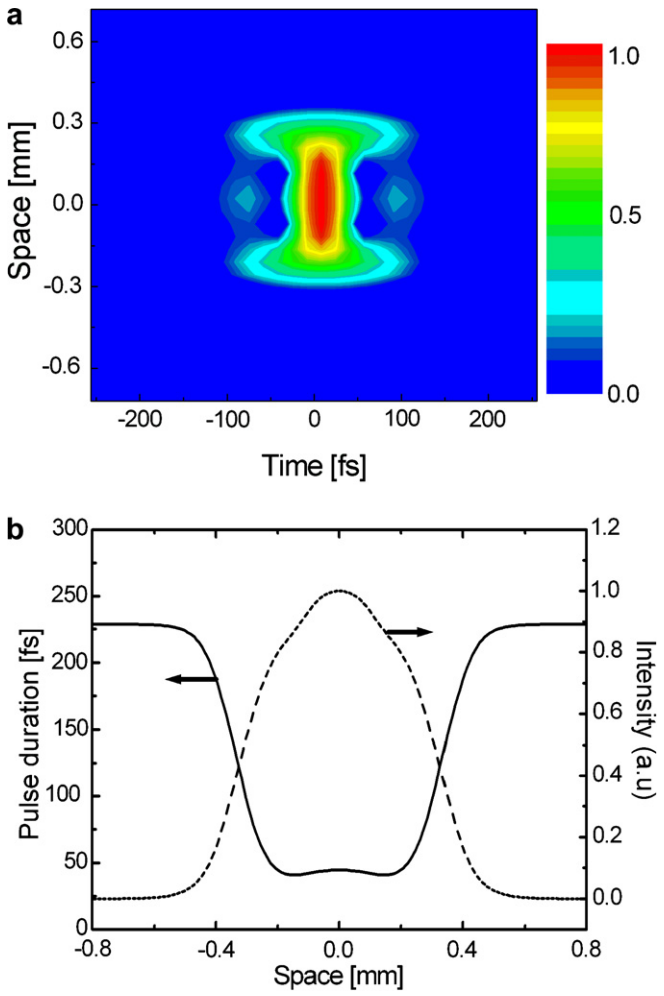

Fig. 5. (a) Calculated spatial–temporal intensity profile of the FF pulse at the exit face. (b) The spatial profile of the averaged pulse duration and the time-integrated intensity of the FF pulse.

earity [5,7]. The shortest pulse duration around the beam center is 45 fs, mainly limited by the competition between cascading and cubic nonlinearities. Fig. 5b shows the pulse duration and the time-integrated intensity estimated at each position across the FF beam. The averaged pulse durations for FF and SH pulses, weighted with the spatial intensity profile, are 48 and 47 fs, respectively. These values are, though only slightly, broader than the duration at the beam center: the compression ratio as a whole beam is degraded by the spatial distribution. On the other hand, it is found that 65% of the total energy is contained within 200 μm from the beam centre and that the pulse duration is almost uniform in this area. This probably comes from the saturable properties of the cascading nonlinearity, and would be advantageous in this bulk-type pulse compressor, in a sense that it leads to spatially-uniform compression.

In order to achieve adiabatic compressions in a rigorous sense, the local wave-vector mismatch should change only gradually along propagation. Then the energy dissipation into the pedestal or into the continuum would be reduced further. In our experiments, we chose the device length of 50 mm, considering the realistic experimental parameters of the confocal length, the beam diameter, and the clear aperture (determined by the device thickness along *c*-axis). A longer device with a waveguide structure is promising for better performances. It will enable the energy confinement in a long distance, leading to lower-power operation, ideal soliton pulses, and spatially-uniform compression.

4. Conclusion

We have demonstrated engineerable compression of two-colored femtosecond pulses in a 50-mm-long linearly-chirped APPMgLN device. Quadratic solitons generated from fundamental input are reshaped through the cascaded parametric interactions. Mutually trapped two-colored pulses of about 55-fs duration with small pedestal are generated from the fundamental pulses at the central wavelength of 1570 nm. We numerically studied the spatio-temporal nonlinear dynamics and found that the temporal profiles are spatially non-uniform, but that the uniformity can be significantly improved due to the saturable nature of the cascading nonlinearity. For an improved operation as an adiabatic soliton compressor, a longer waveguide device is promising. It will enable lower-power operation, generation of ideal soliton pulses with spatial uniformity. Optimization of the QPM grating structure, such as nonlinearly chirped grating may shorten the device length. We believe that the two-colored timing-locked pulses with shorter duration will find new applications in optical information processing or in the light-matter control.

Acknowledgements

This work is partially supported by Japan Society for the Promotion of Science (JSPS), MEXT KAKENHI (20686006) and National Natural Science Foundation of China (Nos. 10704047, 10574092).

References

[1] G.I. Stegeman, D.J. Hagan, L. Torner, J. Opt. Quant. Electron. 28 (1996) 1691.
[2] X. Liu, L.J. Qian, F. Wise, Opt. Lett. 24 (1999) 1777.
[3] S. Ashihara, J. Nishina, T. Shimura, K. Kuroda, J. Opt. Soc. Am. B 19 (2002) 2505.
[4] J. Moses, F.W. Wise, Opt. Lett. 31 (2006) 1881.
[5] M. Bache, J. Moses, F.W. Wise, J. Opt. Soc. Am. B 24 (2007) 2752.
[6] J. Moses, E. Alhammali, J.M. Eichenholz, F.W. Wise, Opt. Lett. 32 (2007) 2469.
[7] C. Menyuk, R. Shiek, L. Torner, J. Opt. Soc. Am. B 11 (1994) 2434.
[8] A.V. Buryak, P. Di Trapani, D. Skryabin, S. Trillo, Phys. Rep. 370 (2002) 63.
[9] L. Torner, A. Barthelemy, IEEE J. Quant. Electron. 39 (2003) 22.
[10] L. Torner, C. Clausen, M. Fejer, Opt. Lett. 23 (1998) 903.
[11] A.V. Buryak, Y.S. Kivshar, Opt. Lett. 19 (1994) 1612.
[12] L. Torner, Opt. Commun. 114 (1995) 136.
[13] S. Carrasco, J. Torres, L. Torner, R. Schiek, Opt. Lett. 25 (2000) 1273.
[14] R. Schiek, R. Iwanow, T. Pertsch, G.I. Stegeman, G. Schreiber, W. Sohler, Opt. Lett. 29 (2004) 596.
[15] G. Valiulis, A. Dubietis, R. Danielius, D. Caironi, A. Visconti, P. Di Trapani, J. Opt. Soc. Am. B 16 (1999) 722.
[16] N.E. Yu, J.H. Ro, M. Cha, S. Kurimura, T. Taira, Opt. Lett. 27 (2002) 1046.
[17] S. Ashihara, T. Shimura, K. Kuroda, J. Opt. Soc. Am. B 20 (2003) 853.
[18] N. Fujioka, S. Ashihara, H. Ono, T. Shimura, K. Kuroda, Opt. Lett. 31 (2006) 2780.
[19] N. Fujioka, S. Ashihara, H. Ono, T. Shimura, K. Kuroda, J. Opt. Soc. Am. B 22 (2005) 1283.
[20] X. Xie, J. Huang, M.M. Fejer, Opt. Lett. 31 (2006) 2190.
[21] S. Ashihara, T. Shimura, K. Kuroda, Nan Ei Yu, S. Kurimura, K. Kitamura, M. Cha, T. Taira, Appl. Phys. Lett. 84 (2004) 1055.
[22] X. Zeng, S. Ashihara, N. Fujioka, T. Shimura, K. Kuroda, Opt. Exp. 14 (2006) 9358.
[23] D. Zelmon, D. Small, D. Jundt, J. Opt. Soc. Am. B 14 (1997) 3319.